Threshold Photoelectron–Photoion Coincidence Spectroscopy of Perfluorocarbons. 1. Saturated Perfluorocarbons C 2 F 6 , C 3 F 8 , and n -C 4 F 10

ARTICLE *in* THE JOURNAL OF PHYSICAL CHEMISTRY A · MAY 1998

Impact Factor: 2.69 · DOI: 10.1021/jp9719016 · Source: OAI

4 AUTHORS, INCLUDING:

Chris Mayhew
Indian Institute of Technology Roorkee
63 PUBLICATIONS **822** CITATIONS

SEE PROFILE

Richard P Tuckett
University of Birmingham
162 PUBLICATIONS **2,057** CITATIONS

SEE PROFILE

Threshold Photoelectron−Photoion Coincidence Spectroscopy of Perfluorocarbons. 1. Saturated Perfluorocarbons C_2F_6, C_3F_8, and *n*-C_4F_{10}

Gary K. Jarvis,[†] Kenneth J. Boyle,[‡] Chris A. Mayhew,[†] and Richard P. Tuckett*[,‡]

Chemical Physics Laboratory, School of Physics and Astronomy, and School of Chemistry, University of Birmingham, Edgbaston, Birmingham, B15 2TT, U.K.

Received: June 10, 1997; In Final Form: February 18, 1998

Using vacuum-ultraviolet radiation from a synchrotron source, threshold photoelectron−photoion coincidence (TPEPICO) spectroscopy has been used to study the decay dynamics of the valence electronic states of three saturated perfluorocarbon cations, $C_2F_6^+$, $C_3F_8^+$, and *n*-$C_4F_{10}^+$, in the energy range 12−25 eV. Electrons and ions are detected by threshold electron analysis and time-of-flight mass spectrometry, respectively, allowing breakdown diagrams showing the formation probability of fragment ions as a function of the internal energy of the parent ion to be obtained. The threshold photoelectron spectra of C_3F_8 and *n*-C_4F_{10} are reported for the first time in the literature. Higher resolution, fixed-energy TPEPICO spectra were also performed on some of the fragment ions, and the translational kinetic energy released in fragmentation was determined. By analysis of the breakdown diagrams of the three ions, nonstatistical effects were observed for states below 18 eV, indicating that decay takes place rapidly from these states before internal energy conversion can occur. This study indicates that impulsive decay can occur even for molecules with up to 14 atoms, implying that statistical decay cannot necessarily be expected even for large molecular species. Analysis of the mean kinetic energy releases also supports the suggestion that impulsive behavior is taking place for the fragmentation of $C_2F_6^+$ into $C_2F_5^+ + F$. For states above 18 eV, it is not obvious from this study whether decay is statistical or not. From the C_3F_8 study, new upper limits for the adiabatic ionization energy of the CF_3 radical (8.8 ± 0.1 eV) and the heat of formation of $C_3F_7^+$ at 298 K (−360 ± 20 kJ mol^{-1}) have been determined.

1. Introduction

Threshold photoelectron−photoion coincidence (TPEPICO) spectroscopy is a well-established technique by which information on the decay dynamics of individual vibronic states of positively charged molecular ions can be obtained. Specifically, this technique enables the formation probability of fragment ions as a function of the internal energy of the excited parent ion, as well as the kinetic energy released into fragment channels, to be determined. These measurements are important guides to determine whether the decay of an excited parent ion occurs impulsively or statistically. For a species to decay statistically, according to RRKM theory,[1] the photoexcited ion must live long enough for several vibrations to take place, and internal conversion to the ground electronic state is assumed to take place so rapidly that dissociation only occurs from this surface. For internal energy conversion to work well, a large number of closely spaced electronic states are needed which is often the case for large polyatomic species. However, in 1965 Lifshitz and Long[2] made mass spectrometric measurements on two saturated perfluorocarbon (PFC) molecules, C_2F_6 and C_3F_8. They showed that the high yield of $C_2F_5^+$ and $C_3F_7^+$ caused by C−F bond breakage compared to that of CF_3^+ caused by C−C bond breakage at low electron energies could not be modeled by RRKM theory. They suggested that direct, impulsive decomposition from excited electronic states of the parent ion was occurring, without prior internal conversion of electronic into vibrational energy of the ground state. These conclusions for C_2F_6 were later confirmed by coincidence experiments using both He I (21.2 eV)[3,4] and monochromatized vacuum-UV (VUV) radiation from 13 to 20 eV.[5] It has remained a surprise that these saturated PFC cations, including the first member of the series, CF_4^+,[6] do not behave statistically, especially since their analogous hydrocarbon cations do fragment in a statistical manner.[7,8] In this paper, a complete study of three saturated PFCs, C_2F_6, C_3F_8, and *n*-C_4F_{10}, by TPEPICO spectroscopy is presented. A second paper[9] presents results for three unsaturated PFCs, C_2F_4, C_3F_6, and 2-C_4F_8, with one cyclic PFC, c-C_4F_8, included for comparison. In these studies, VUV radiation from a synchrotron is used as the photoionization source. The advantage of using synchrotron radiation is that photoionization and decay behavior can be investigated at energies greater than 21.2 eV, thus accessing valence orbitals beyond this energy. We report the first observations of threshold photoelectron spectra (TPES) for C_3F_8 and *n*-C_4F_{10} and state-selected coincidence results for their parent ions. As the size of molecule is increased, it is expected that statistical behavior will start to dominate as the density of states escalates. An aim of this study is to determine how true this hypothesis is.

2. Experimental Section

The apparatus for performing the TPEPICO experiments has been described in detail elsewhere.[6,10,11] VUV photons were energy selected over the range 10−30 eV using a 1 m Seya monochromator at the Daresbury Laboratory synchrotron radiation source. The monochromatized light is admitted into an interaction region through a capillary, and the photon flux is monitored using a photomultiplier tube attached via a Pyrex window coated on the inside with sodium salicylate. A 20 V

* Author for correspondence: e-mail r.p.tuckett@bham.ac.uk; fax:UK +121 414 4426.
[†] School of Physics and Astronomy.
[‡] School of Chemistry.

S1089-5639(97)01901-4 CCC: $15.00
Published on Web 04/17/1998

cm^{-1} field draws electrons from the interaction region to a threshold electron analyzer. By the tuning of a cylindrical electrostatic lens designed with large chromatic aberrations and a 127° postanalyzer, energetic electrons are rejected on axis, and only electrons with essentially zero kinetic energy reach the channeltron electron multiplier. The theoretical half width at half-maximum of the detector is 10 meV,[11] but the presence of the hot electron tail extending to ca. 160 meV[6] will, to some extent, degrade this resolution. Positive ions are extracted from the interaction region by the field and are drawn toward the ion detector through a linear time-of-flight (TOF) mass spectrometer. The ion drift tube consists of a two-stage acceleration region configured to satisfy the space focusing condition[12] and a field-free region of length 186 mm. This configuration allows sufficient TOF resolution for kinetic energy releases from a dissociative ionization process to be measured, while still maintaining a high collection efficiency. The ion signal is recorded using a pair of microchannel plates (MCPs) with a radius of 2 cm in a chevron formation. The sensitivity of the MCPs decreases with increasing mass, and over the large mass range of ions detected, CF^+ through to $C_4F_9^+$, the sensitivity decreases by a factor of ca. 10. More details are given in section 4.3. Pulses from the electron and ion detectors pass via discriminator and pulse shaping circuits to a time-to-digital converter configured in the multihit mode. The electrons provide the start and the ions provide the stop pulses, enabling signals from the same ionization event to be detected in delayed coincidence.

TPEPICO spectra can be recorded either continuously as a function of photon energy or at a fixed energy. Since the arrival time of the ions is related to their mass, it is possible to deduce the (fragment) ions that are formed at any particular energy. In the energy-scanning mode, all the ions produced are recorded, and hence the TOF resolution is correspondingly low. Breakdown diagrams can be calculated from these data by dividing the number of coincident ions of a given mass at any particular energy by the total number of ions at that energy. This gives the formation probability of the product ions as a function of the internal energy of the excited parent ion.

Fixed-energy TOF spectra are recorded, generally at energies corresponding to peaks seen in the scanning TPEPICO plots, using a TOF resolution as high as the signal level permits. Fragment ions often have enough translational energy released for the peaks to be substantially broadened. It is then possible to obtain kinetic energy release distributions (KERDs) and hence mean kinetic energy releases from analysis of the TOF shapes.[13] The method used is to compute a set of TOF peaks, each with a discrete energy release $E_T(n)$. The discrete energies are calculated by $E_T(n) = ((2n - 1)^2)\Delta E$ where $n = 1, 2, 3, ...$, and ΔE depends primarily on the statistical quality of the data. Taking each computed peak calculated at energy $E_T(n)$ to be a reasonable representation of the release from energies $4(n - 1)^2\Delta E$ to $4n^2\Delta E$, a probability can be set to each band centered at $E_T(n) + \Delta E$. This probability is varied by a linear regression technique until the least-squared errors between the simulated and the experimental TOF peak are minimized. Although this technique allows us to obtain a KERD, in practice only mean kinetic energy releases can reliably be obtained in our apparatus.[14]

In the energy-scanning mode, total ion and electron signals are also recorded, providing ion yield curves and TPES, respectively. TPES can also be recorded separately in a noncoincidence experiment, allowing us to calibrate the monochromator by using the ionization of Ar into its $^2P_{1/2}$ ionic state (15.937 eV[15]). In all these experiments, second-order radiation from the grating of the Seya monochromator was not a problem since the ground electronic states of $C_2F_6^+$ etc. occur at energies above that where second-order effects are significant. More importantly, electronic states of $C_2F_6^+$ etc. do not exist at energies of 25−26 eV, twice the energy of the ground states of these ions. Therefore, even if it were present, second-order radiation would not cause problems in these experiments.

The sample gases C_2F_6, C_3F_8, and n-C_4F_{10} were obtained commercially (Fluorochem Ltd., UK), having stated purities of >99%, 97%, and 97%, respectively. They were used without further purification.

3. Theoretical Considerations

3.1. Theoretical Calculation of Breakdown Diagrams. If a molecular ion dissociates statistically, then the breakdown diagram can be reproduced by a theoretical calculation based on transition-state theory. In statistical decay, randomization of the internal energy of the parent ion occurs after several vibrations. The internal energy is thus rapidly converted into vibrational energy of the electronic ground state of the parent ion. Where transition-state theory starts to fail is when the removal of an electron has particular influence on a localized bond, and the parent ion may then dissociate along a specific potential energy surface. A recent example of this behavior has been observed for the fragmentation channels of excited states of CF_3Cl^+ and CF_3Br^+.[16] This type of decay is often termed impulsive. Alternatively, if an excited state of the parent ion has no states that are able to interact with it, radiative transitions may take place instead of energy randomization. An example of this is seen for the fragmentation of the $\tilde{C}\ ^2T_2$ and $\tilde{D}\ ^2A_1$ excited states of CF_4^+.[6]

Statistically, the rate constant for each dissociative process depends on its total energy, E, with each process being characterized by a minimum value E_0 for which the rate constant has its minimum nonzero value. In RRKM theory this has been shown to be equated to[1]

$$k(E) = \frac{\alpha G^*(E - E_0)}{hN(E)} \qquad \text{(I)}$$

where $N(E)$ is the number of quantum states per unit energy for the excited ion, $G^*(E-E_0)$ is the total number of states of the transition state at energy $(E - E_0)$, and α is a statistical factor that determines the reaction path degeneracy. By comparison of the relative rates of dissociation for different product channels, it is therefore possible to formulate breakdown diagrams by comparison of $\alpha G^*(E-E_0)$ for each channel. Due to a lack of information on the moments of inertia of the transition states involved, only vibrational levels were considered. We assume that the effects of rotation into the different product channels which involve a simple bond breakage will approximately cancel, thus reducing any error that may arise from neglecting rotation. The sum of vibrational states at energy E is given by[1,17]

$$G_v(E) = \frac{(E + aE_z)^v}{\Gamma(v + 1)\prod_{i=1}^{v} h\nu_i} \qquad \text{(II)}$$

where ν_i are the vibrational frequencies, E_z is the zero-point energy, v is the number of vibrational frequencies of the transition state, and a is a factor slightly less than 1 that is a function of energy.[17] It should be noted that this approach

depends critically upon the accuracy of the estimates made for the vibrational frequencies of the transition state.

3.2. Calculation of the Kinetic Energy Released in Fragmentation. A photoexcited molecular ion that decays statistically is long-lived on the time period of rotational and vibrational motion. The excess energy is partitioned among the available degrees of freedom, resulting in a relatively low kinetic energy (KE) release as a fraction of the available energy. Alternatively, if the photoexcited parent ion decays impulsively, all of its internal energy may be localized in one bond, allowing a greater fraction of the excess energy to be partitioned into KE of the products. When this is the case, it is easy to differentiate the two extreme types of behavior from the KE released in fragmentation. However, it should be noted that impulsive decay can also result in a low KE release (see below), and therefore when a small release is observed, interpretation of the decay mechanism is more difficult. When decay is of the form $ABC^+ \rightarrow AB^+ + C$, where C is an atom, we can calculate the statistical limit of the kinetic energy released and use this as another method to determine how the parent ion is behaving. For statistical decay, Klots[18] showed that the mean translational energy released in fragmentation, $\langle E_T \rangle$, can be formulated as

$$E_{\text{avail}} = \frac{r-1}{2}\langle E_T \rangle + \langle E_T \rangle + \sum_i \frac{h\upsilon_i}{\exp(h\upsilon_i/\langle E_T \rangle) - 1} \quad \text{(III)}$$

where E_{avail} is the photon energy minus the energy of the $ABC \rightarrow AB^+ + C$ dissociative ionization channel, r is the number of rotational degrees of freedom, and υ_i are now the vibrational frequencies of the AB^+ product. When decay is of the form $(AB-CD)^+ \rightarrow AB^+ + CD$, statistical theory can approximately be shown to produce a mean kinetic energy equivalent to $E_{\text{avail}}/(x+1)$,[19] where x is the number of vibrational degrees of freedom of the transition state. In reality, this model often underestimates the KE release, although it can be used to provide a lower limit.

For an impulsive decay, several models exist that, for conceptual simplicity, can be classified into two distinct categories: interfragment and intrafragment.[20] In the interfragment mechanism, the changes in the potential surface from the initial to the final state produce forces and torques between the fragments. The interfragment mechanism is further divided into a pure impulsive and a modified impulsive model. In the former, the two atoms surrounding the breaking bond recoil so rapidly that initially the rest of the decaying species can be regarded as a spectator. For a pure impulsive model of the kind $(ABC-D)^+ \rightarrow ABC^+ + D$, where C and D are atoms and AB may be polyatomic, momentum is passed to the C atom which in turn interacts with the rest of the fragment, imparting vibrational and rotational energy to it. E_{avail} and $\langle E_T \rangle$ can be shown to be related by[20]

$$\frac{\langle E_T \rangle}{E_{\text{avail}}} = \frac{\mu_{C,D}}{\mu_{ABC,D}} \quad \text{(IV)}$$

where $\mu_{C,D}$ is the reduced mass of the C−D breaking bond and $\mu_{ABC,D}$ is the reduced mass of the two fragments that are formed. In the modified impulsive model, the repulsion is considered to be gentle enough that the remaining bonds stay vibrationally unchanged. In this case, B−C can be regarded as being rigid which results in an even higher fractional energy release since the fragment is only allowed to lose its energy to rotation of ABC^+ and translation of $ABC^+ + D$. Note that both interfragment models predict a relatively high fractional KE release which depends only on the kinematics of the particular photofragmentation and not on the detailed topology of the potential energy curves. These limiting equations of statistical and impulsive decay have been developed for dissociation of a triatomic molecule/ion to a diatomic and an atom. However, in this paper we have applied them to more complex systems where, in addition, both fragments may be molecular.

For the intrafragment case, Mitchel and Simons[21] developed a model to explain vibrational excitation of photofragments following impulsive decay. This can be explained most easily by example. Consider the molecule ABC that is photoexcited to $ABC^{+}*$, which then decays to $AB^+ + C$. If the A−B bond length is considerably changed in $ABC^{+}*$ compared to ABC, a vertical transition from the ground state of the neutral will result in vibrational excitation of this bond. Furthermore, if the dissociation process is adiabatic, and if the A−B bond length is different in AB^+ from $ABC^{+}*$, the AB^+ fragment will also be formed with vibrational excitation. Hence, the fraction of energy available for translational release is reduced. Notice that an intrafragment mechanism of this kind is crucially dependent on the potential energy surface(s) involved. In reality, direct dissociation can take place by a combination of interfragment and intrafragment mechanisms, and almost any fractional translational energy release can be predicted. This conclusion therefore indicates that a low fractional release of kinetic energy does not necessarily mean that decay is proceeding statistically. On the other hand, if a large fractional release is observed, decay is likely to be of an impulsive nature. Finally, it should be noted that statistical decay proceeding via a barrier in the exit channel can also lead to a relatively large fractional KE release. However, since all the fragment ions from which we measure a KE release in this paper can arise from single bond-breaking channels that involve loose transition states, we assume this process to be unlikely.

4. Results

4.1. TPES of C_2F_6, C_3F_8, and *n*-C_4F_{10}. The TPES of C_2F_6 and C_3F_8 in the range 13.0−24.8 eV and of *n*-C_4F_{10} in the range 12.0−26.0 eV at a resolution of 0.4 nm are shown in the lower panels of Figures 1−3, respectively. The breakdown diagrams are also shown in the figures and will be discussed later. The three TPES have many similar features, notably with respect to the relative intensity and spacing of the peaks. For all three spectra, two clusters of relatively intense features between 16 and 19 eV and 20−23 eV, corresponding to excited ionic states, and a much weaker peak between 13 and 15 eV, corresponding to ionization to the ground state, are observed. The only notable difference occurs for *n*-C_4F_{10} which, apart from having less well resolved features, has an extra unresolved feature between 14 and 16 eV of approximately the same intensity as the ground-state peak.

These similarities strongly suggest that electrons are being removed from orbitals that have a similar bonding character at comparable excitation energies in these three molecules. As the size of the PFC increases, the increase in the density of electronic states that must occur has only a limited effect on the TPES. Therefore, the spectra of C_3F_8 and *n*-C_4F_{10} can, in part, be interpreted by comparison with that of C_2F_6 for which more information on the nature of its molecular orbitals is known. For example, the ground state of $C_2F_6^+$ has symmetry $^2A_{1g}$, which corresponds to the loss of a C−C σ-bonding electron.[3] It is therefore likely that for C_3F_8 and *n*-C_4F_{10} the highest-occupied molecular orbital is also a C−C σ-bonding orbital. Similarly, since the first excited state of $C_2F_6^+$, $\tilde{A}\ ^2E$,

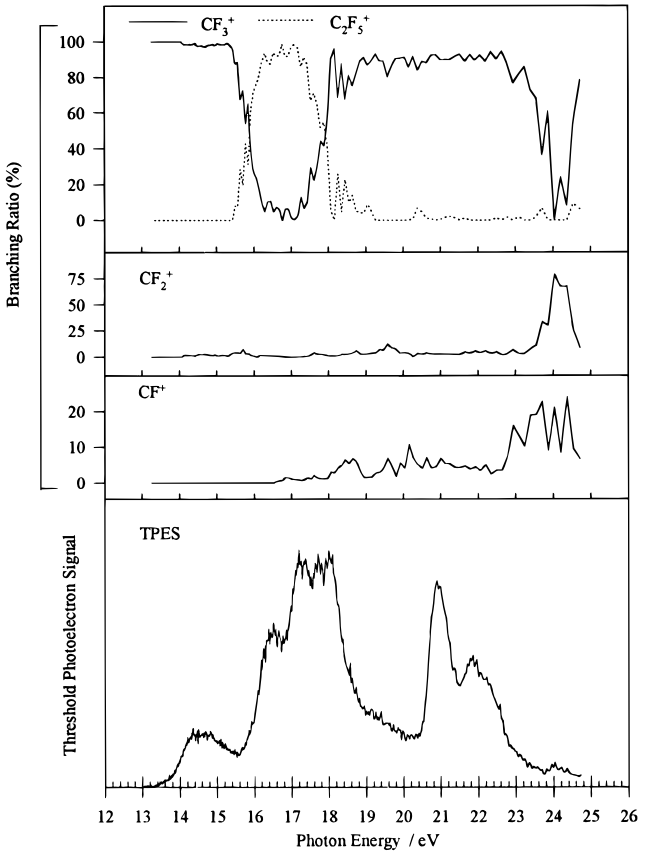

Figure 1. Threshold photoelectron spectrum (lower panel) and the corresponding breakdown diagram (upper panels) for C_2F_6. In both cases, the optical resolution is 0.4 nm, but the step size is 0.1 nm (TPES) and 0.352 nm (breakdown diagram). Mass discrimination effects (Table 1) have been accounted for in the breakdown diagram, and false coincidences were removed from the 3-dimensional coincidence map.

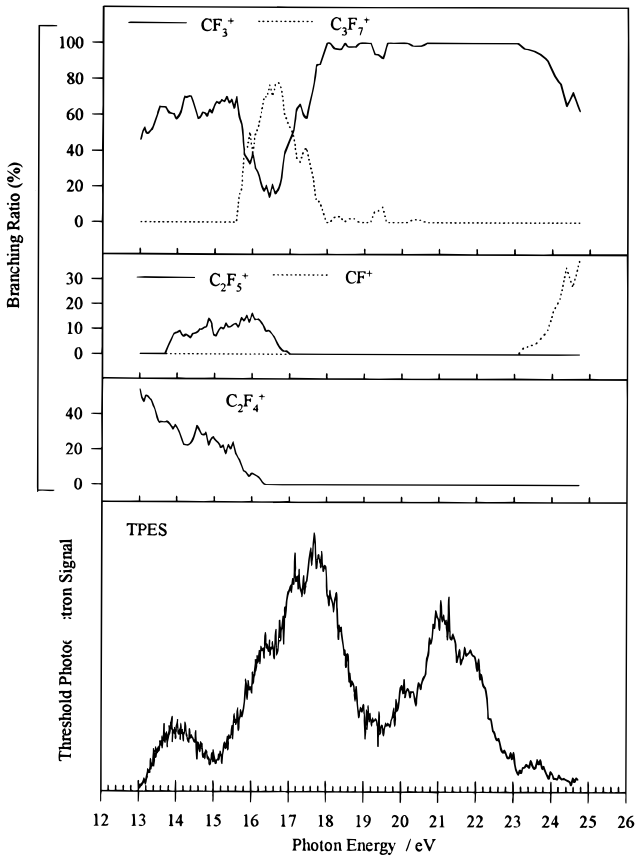

Figure 2. Threshold photoelectron spectrum (lower panel) and the corresponding breakdown diagram (upper panels) for C_3F_8. In both cases, the optical resolution is 0.4 nm, but the step size is 0.1 nm (TPES) and 0.352 nm (breakdown diagram). Mass discrimination effects (Table 1) have been accounted for in the breakdown diagram, and false coincidences were removed from the 3-dimensional coincidence map.

corresponds to the loss of an electron from a degenerate orbital that is largely associated with the 2pπ levels on the fluorine atoms,[3] it seems plausible that states occurring in this region for the longer-chain PFCs might also correspond to electron loss from a similar orbital. The extra peak in the *n*-C_4F_{10} spectrum between 14 and 16 eV could arise due to the presence of a different C−C orbital, since this molecule, unlike C_2F_6 or C_3F_8, has two kinds of C−C bond.

The observed onset of ionization into the ground ionic state for these molecules decreases with increasing chain length. For C_2F_6, C_3F_8, and *n*-C_4F_{10} this onset occurs at 13.4 ± 0.1, 13.0 ± 0.1, and 12.6 ± 0.1 eV, respectively.[22] For C_2F_6 our value is in good agreement with that recorded previously.[5] For C_3F_8, however, our value is ca. 0.2 eV lower than that measured by Noutary[23] and ca. 0.4 eV lower than that recorded by Lifshitz et al.,[24] who used photoionization mass spectrometry (PIMS) and retarding potential difference electron impact (RPD EI) ionization, respectively, to determine these values. Noutary also recorded the ionization thresholds for the production of positive ions in *n*-C_4F_{10} and observed an onset of 13.05 eV, again ca. 0.4 eV higher than our value.

The TPES of C_2F_6 below 21.2 eV as recorded by Inghram et al.[5] agrees extremely well with the one shown in Figure 1. This energy was the maximum of their range, since they used the Hopfield afterglow continuum as a light source. On comparison with the He I PES obtained by Simm et al.,[3] the main difference is that the largest peak at 17.2 eV appears greatly enhanced under threshold conditions in the TPES. This enhancement in intensity could be due either to autoionization effects or to a change in the relative cross section between excitation at threshold (17.2 eV) and with He I (21.2 eV) radiation. As explained in the following section, we believe the former explanation to be the case. To the authors' knowledge, no previous photoelectron spectra of C_3F_8 or *n*-C_4F_{10} have been published.

4.2. Total Ion Yield Curves. While recording threshold photoelectron spectra at a resolution of 0.4 nm with a step size of 0.1 nm, the total ion signal is also collected, providing a measurement of the total ion production at any particular energy. The total ion yield curves for C_2F_6, C_3F_8, and *n*-C_4F_{10} are shown in Figures 4−6, respectively. The ion yield curve gives a representation of the relative photoionization cross section across the energy range. At an energy, *E*, the cross section represents the effects of ionization from the state(s) at *E* as well as from lower ionic states. These lower states release electrons of kinetic energy greater than zero. In TPES the relative photoionization cross section is also revealed but only gives the cross section under threshold conditions, and the effects of ionization from the lower-lying states are removed. If the cross section to any particular state remains unchanged in moving from threshold to nonthreshold conditions, then the total ionization cross section should be equivalent to the integral of the ionization cross section to each state, reflected in the TPES, from the onset of ionization to energy, *E*. Thus, by progressively summing the TPES signal from threshold to *E*, if the basic assumption stated above is true, the normalized ion yield curve should be reproduced. Figures 4−6 also show the "summed" TPES, and it appears that the ion yield curve and the summed TPES for

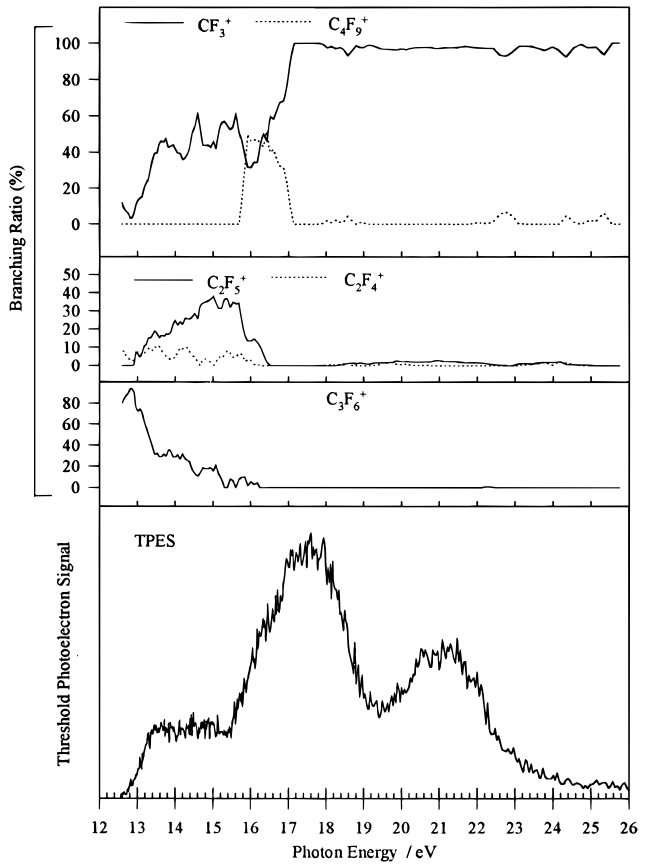

Figure 3. Threshold photoelectron spectrum (lower panel) and the corresponding breakdown diagram (upper panels) for *n*-C_4F_{10}. In both cases, the optical resolution is 0.4 nm, but the step size is 0.1 nm (TPES) and 0.393 nm (breakdown diagram). Mass discrimination effects (Table 1) have been accounted for in the breakdown diagram, and false coincidences were removed from the 3-dimensional coincidence map.

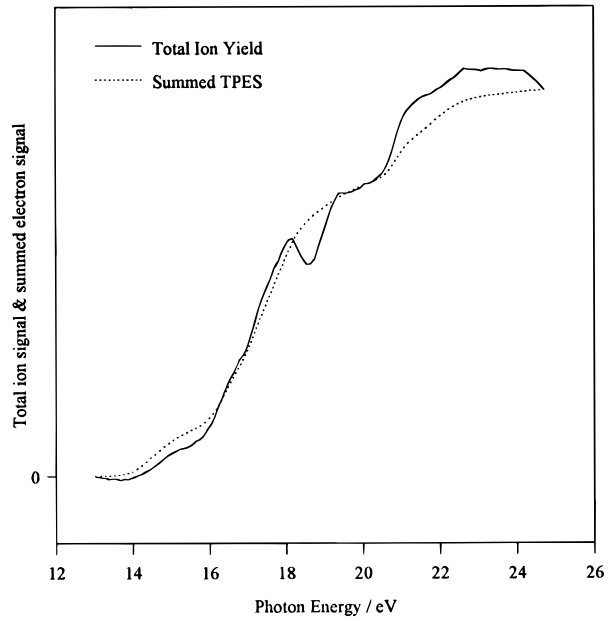

Figure 4. Total ion yield and summed TPES signal for C_2F_6 as a function of energy. The summed TPES signal at energy *E* is the integral of the individual TPES channels from threshold to *E*.

C_2F_6, C_3F_8, and *n*-C_4F_{10} do mimic each other over a wide range of energies, particularly from threshold to ca. 18 eV. Differences observed between these two curves can help to understand the types of ionization process that are occurring.

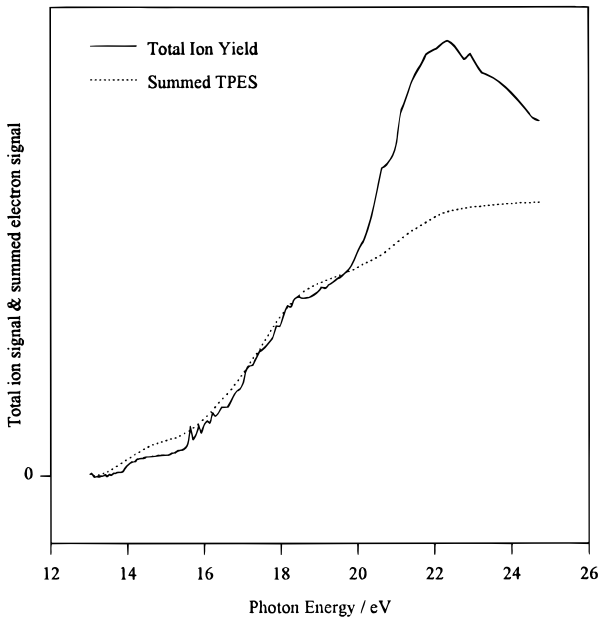

Figure 5. Total ion yield and summed TPES signal for C_3F_8 as a function of energy. The summed TPES signal at energy *E* is the integral of the individual TPES channels from threshold to *E*.

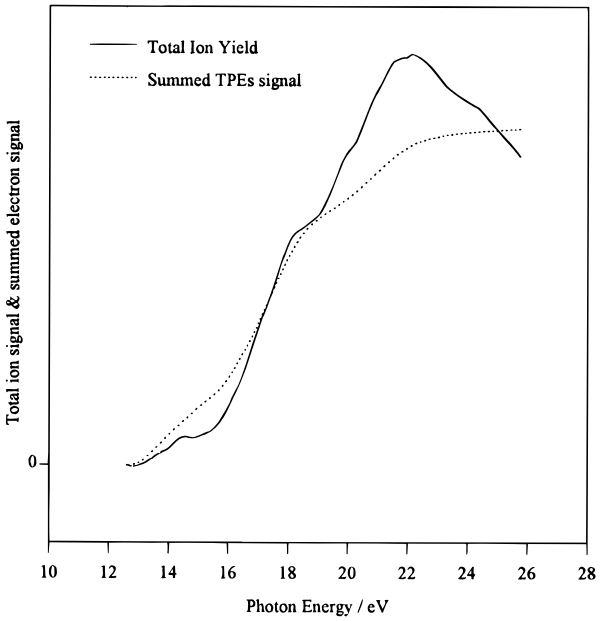

Figure 6. Total ion yield and summed TPES signal for *n*-C_4F_{10} as a function of energy. The summed TPES signal at energy *E* is the integral of the individual TPES channels from threshold to *E*.

The agreement between the two curves for C_2F_6 is extremely good up to ca. 18 eV (Figure 4). At this energy, there is a disparity between the two curves. Whether this is seen as a peak at 18 eV or a dip at 18.5 eV in the ion yield relative to the integrated TPES depends primarily on how the two curves are normalized. In both cases, however, this difference indicates that autoionizing states of C_2F_6 are present in the region around 18 eV. These states may emit electrons in the energy range from zero up to the photon energy minus the energy of the state to which autoionization occurs. Therefore, if some electrons emitted are of zero or near-zero energy, extra peaks will appear in the TPES. This interpretation agrees well with the difference in relative intensity of the 17.2 eV peak under threshold and He I conditions (see section 4.1). At energies in excess of this

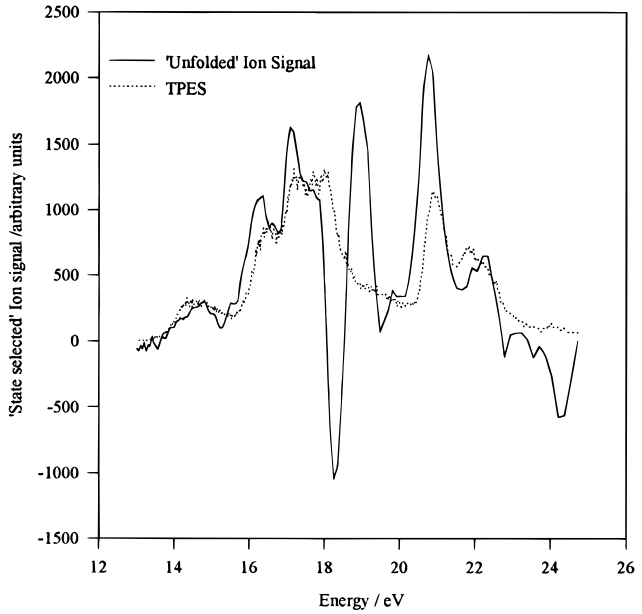

Figure 7. "Unfolded" ion yield and TPES for C_2F_6 (see section 4.2 of text).

feature, the ion yield curve should merely continue the trend observed in the summed TPES. However, the ion yield curve undergoes a further rise before leveling off by 19.5 eV. This rise may be due to an increase in the photoionization cross section to the lower-energy states of $C_2F_6^+$ in the energy range 18−20 eV. Note that, as no decrease in the ion yield occurs above this energy range, it is unlikely that autoionization is responsible for this rise. At 20.5 eV the ion yield shows a further rise compared to the summed TPES. This energy corresponds to the threshold of the peak at 21 eV seen in the TPES. This rise again may be due to an increase in the photoionization cross section to the lower-energy states. Why this cross section should rise suddenly at an energy similar to a peak in the TPES is not clear, although a similar phenomenon occurs around 20 eV for C_3F_8 and *n*-C_4F_{10} (Figures 5 and 6). Unlike C_2F_6, no sharp decline in the ion yield curve occurs at any energy for C_3F_8 or C_4F_{10}. This indicates that Rydberg states are not responsible for peaks in the TPES via autoionization mechanisms. For all three species, a decline in the ion yield occurs for energies above that of the highest valence orbital (>24 eV), indicating a reduction in the photoionization cross section to the valence states. It should be pointed out, however, that mass discrimination of the TOF mass spectrometer may also play a role in causing deviations between the summed TPES and the ion yield curves since the MCPs detect heavy mass ions with lower efficiency than lighter ions (see section 4.3). Unfortunately, this effect is difficult to quantify since this experiment gives no information on the mass of the ions contributing to the ion yield.

Another method of presenting these trends is to perform the inverse of that presented above. That is, starting from high energy, each channel can be subtracted from the following channel of a total ion yield curve to produce a plot that should resemble the TPES in many respects and be state selective. This is shown in Figure 7 for C_2F_6. Negative peaks reflect either a change in cross section or the presence of Rydberg states which lie at energies slightly below the observed feature. Sharp positive peaks reflect a fast change in cross section. Note the presence of the negative peak at 18.2 eV and the positive peaks at 14.5, 16.0, 17.0, and 20.7 eV that correspond to peaks seen in the TPES.

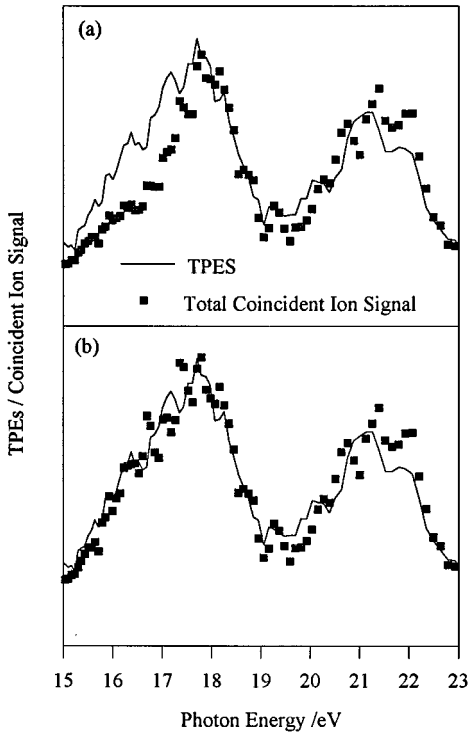

Figure 8. Total coincident ion signal and the normalized TPES for C_3F_8, demonstrating mass discrimination effects over the range 15−23 eV: (a) raw data, (b) $CF_3^+ \times 1$, $C_2F_5^+ \times 1.9$, $C_3F_7^+ \times 3.5$.

4.3. Fragmentation of the Valence States of $C_2F_6^+$, $C_3F_8^+$, and *n*-$C_4F_{10}^+$. TPEPICO spectra in the energy-scanning mode were recorded from 13.0 to 24.8 eV with a constant step size of 0.352 nm for C_2F_6 and C_3F_8 and from 12.4 to 26.0 eV with a step size of 0.393 nm for *n*-C_4F_{10}. The optical resolution of the Seya monochromator was set at 0.4 nm for all of these measurements. Following an initial analysis of the data, it became clear that mass discrimination effects could not be ignored, especially for the fragments observed from $C_3F_8^+$ and *n*-$C_4F_{10}^+$. This was seen by summing the total ion signals at each energy and plotting them with the TPES which was normalized so that signal intensities could be compared. Since each ionization event results in the production of an electron and an ion, the summed coincident ion signal should match the TPES in shape and detail. However, as illustrated in Figure 8a which shows the TPES and the total coincident ion signal (the sum of coincident ion signals for all the fragment ions) for photoionization of C_3F_8 between 15 and 23 eV, it is obvious that this is not the case. The major difference occurs between 15.5 and 18.0 eV where $C_3F_7^+$ is a major fragment (see Figure 2). The best match between the TPES and the summed coincident ion signal is shown in Figure 8b. It was obtained when the $C_3F_7^+$ signal was multiplied by a factor of 3.5 and the $C_2F_5^+$ by a factor of 1.9 relative to the CF_3^+ signal, thus accounting for the mass discrimination of the MCPs which favors the lighter mass ions. [Discrimination of the MCPs due to the kinetic energy released in fragmentation was assumed to be negligible for the following reason. Taking the fragmentation of $C_2F_6^+$ into $C_2F_5^+$ and F as an example, the maximum total KE released is seen to be 1.25 eV (Table 3), meaning that only 0.17 eV is given to the $C_2F_5^+$ fragment. This energy corresponds to a velocity of 528 m s^{-1}. So, in a drift time of ca. 20 μs, ions ejected perpendicular to the spectrometer will only travel a distance of 1.06 cm, well within the reactive area of the MCPs (radius 2 cm). Furthermore, we calculate that the maximum energy of a fragment ion, irrespective of its mass, before

TABLE 1: Factors Used To Account for Mass Discrimination of the Observed Fragment Ions

ion	mass (amu)	multiplication factor	ion	mass (amu)	multiplication factor
CF^+	31	0.6	$C_2F_5^+$	119	1.9
CF_2^+	50	0.8	$C_3F_6^+$	150	2.7
CF_3^+	69	1	$C_3F_7^+$	169	3.5
$C_2F_4^+$	100	1.5	$C_4F_9^+$	219	6.4

TABLE 2: Dissociation Channels and Appearance Energies of Ions Formed from C_2F_6, C_3F_8, and *n*-C_4F_{10}

parent molecule	dissociation channel	dissociation energy/eV	appearance energy/eV[a]
C_2F_6	$C_2F_5^+ + F$	14.74	15.4(0.1)
	$CF_3^+ + CF_3$	12.89	13.4(0.1)
	$CF_2^+ + CF_4$	13.53	14.0(0.2)
	$CF_2^+ + CF_3 + F$	19.27[b]	
	$CF^+ + CF_4 + F$	16.81[c]	16.6(0.5)
	$CF^+ + CF_3 + 2F$	22.55[b]	
C_3F_8	$C_3F_7^+ + F$	16.05[c]	15.4(0.2)
	$C_2F_5^+ + CF_3$	13.71[c]	13.6(0.2)
	$C_2F_4^+ + CF_4$	12.07	13.0(0.1)
	$C_2F_4^+ + CF_3 + F$	17.81[b]	
	$CF_3^+ + C_2F_5$	12.96	13.0(0.1)
n-C_4F_{10}	$C_4F_9^+ + F$	14.95	15.7(0.3)
	$C_3F_6^+ + CF_4$	11.16	12.6(0.1)
	$C_3F_6^+ + CF_3 + F$	16.90	
	$C_2F_4^+ + C_2F_6$	11.26	12.6(0.4)
	$C_2F_4^+ + C_2F_5 + F$	16.74	
	$C_2F_5^+ + C_2F_5$	12.64	13.0(0.4)
	$CF_3^+ + C_3F_7$	12.34	12.6(0.4)

[a] Appearance energies were determined from their first onset. Errors are given in parentheses. [b] These values are given in addition to the lowest dissociation energy channel in cases where F^- transfer can take place. [c] In these three cases, the calculated dissociation energies lie above experimentally determined appearance energies, implying error(s) in thermochemical data.

discrimination has to be accounted for is as large as ca. 0.6 eV.] The mass discrimination procedure was performed on all the observed fragment ions until a reasonable match was obtained for the three molecules. The factors shown in Table 1 were used to account for the observed discrimination effects. Using these multiplying factors, the ions observed and corresponding breakdown diagrams are shown in the upper panels of Figures 1−3. Threshold photoelectron spectra were recorded simultaneously in these energy-scanning experiments, although since these spectra used a larger step size to that used in the previously mentioned TPES it is the latter spectra that are displayed in the lowest panel of the Figures.

The experimentally determined appearance energies and corresponding possible dissociation energies for all of the fragment ions produced from $C_2F_6^+$, $C_3F_8^+$, and *n*-$C_4F_{10}^+$ are shown in Table 2. These appearance energies were determined from their first onset. We assume that the effects of the high-energy tail of the internal energy of the neutral to be small, because many of the ionization processes in these PFCs are impulsive with low Franck−Condon factors at threshold. The majority of thermochemical data to determine the dissociation energies were taken from Lias et al.[25] However, the heats of formation of *n*-C_4F_{10} and C_3F_7 were taken from Bryant,[26] of $C_3F_7^+$ from Su et al.,[27] and of CF_3^+ from Tichy et al.[28] All these heats of formation are for 298 K and use the "stationary electron" convention to define the heat of formation of a cation.[29] While it is possible and indeed common for appearance energies to be greater than dissociation energies in nonstatistical fragmentation, the appearance energy can never lie below the dissociation energy. Inconsistencies between the appearance energies and the lowest possible dissociation energies of three decay channels are obvious, indicating possible errors in the thermochemical data used (especially the heat of formation of $C_3F_7^+$). We have used the procedure given in Traeger et al.[29] to relate an appearance energy (i.e. the first onset) of a fragment cation at a temperature *T* to the heat of formation of that cation at the same temperature. From the $AE(C_3F_7^+/C_3F_8)_{298}$ value of 15.4 ± 0.2 eV, and allowing for the calculated internal energy of $C_3F_7^+$ at 298 K, we obtain a new upper limit for the heat of formation of this ion at this temperature of −360 ± 20 kJ mol^{-1}.

For all three systems studied, no parent ions are formed at any photon energy. The most likely reason is that, as with CF_4,[6] the ground states of the parent ions are repulsive in the Franck−Condon region accessible by one-photon excitation. Thus, all three PFCs possess dissociative ionization channels below the observed onset of ionization. Statistical break-up relies on the fact that the excess energy is transferred to vibrational energy of the ground state of the parent ion. Therefore, when the ground ionic state is repulsive, nonstatistical behavior will result.

4.3.1. Fragmentation in the Range 12−15 eV. We first consider the fragmentation of the ground states of the PFC cations between 12 and 15 eV. Our results show that the ground state of $C_2F_6^+$ produces CF_3^+ exclusively, whereas the ground state of $C_3F_8^+$ and *n*-$C_4F_{10}^+$ have at least two dissociative channels. For $C_2F_6^+$, the calculated $CF_3^+ + CF_3$ dissociation energy lies 0.5 eV below the onset of photodissociative ionization, and this channel is the only one that is energetically open. Fragmentation to CF_3^+ is compatible with the ground state of $C_2F_6^+$ being formed by electron removal from a C−C σ-bonding orbital.[3] For C_3F_8, the principal fragments are $C_2F_4^+$ and CF_3^+, with both having appearance energies of 13.0 ± 0.1 eV. Furthermore, $C_2F_5^+$ has an appearance energy only slightly higher, 13.6 ± 0.2 eV, and has a small percentage of the total branching ratio up to about 17 eV. For *n*-C_4F_{10}, $C_3F_6^+$ accounts for the largest fraction of ions formed at threshold and, as with C_3F_8, CF_3^+ is also a major product. The percentage yield of $C_2F_4^+$ from C_3F_8 and $C_3F_6^+$ from *n*-C_4F_{10} decreases from the observed onset of ionization, and in both cases the yield of CF_3^+ increases. The creation of $C_2F_4^+$ and $C_3F_6^+$ at these energies is especially interesting, since their production is only thermodynamically possible if intramolecular rearrangement involving the migration of a fluorine anion occurs in the transition state to form CF_4 as the sole neutral fragment (Table 2). Since the ground states of these three PFC cations are assumed to be repulsive in the Franck−Condon region, decay probably takes place rapidly in a time period of one vibration or less. In support of this, Inghram et al. found by field ionization methods that CF_3^+ was formed from C_2F_6 in less than 5×10^{-13} s.[5] Decay is therefore likely to be impulsive, and the fragment ions observed should reflect the type of orbital from which an electron is ejected upon ionization. If this orbital is C−C σ-bonding, as expected by comparison with C_2F_6, this explains the presence of CF_3^+ and $C_2F_5^+$ from fragmentation of $C_3F_8^+$. A possible mechanism for the production of $C_2F_4^+$ from $C_3F_8^+$ is shown below:

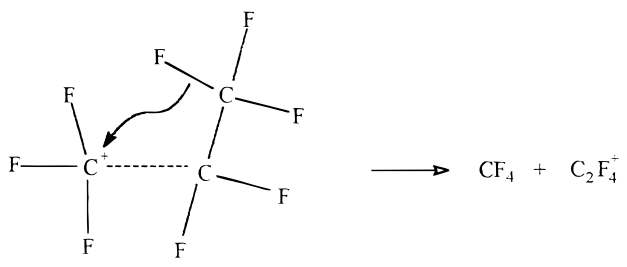

This process depends on F^- migration taking place more rapidly

TABLE 3: Comparison of Mean Total Kinetic Energy Releases Calculated from Experimental Results and from Statistical and Impulsive Dissociation Models[a]

					fraction		
parent ion	daughter ion	$h\nu$/eV	E_{avail}/eV	total $\langle E_T \rangle$/eV[b]	expt[b]	statistical	purely impulsive
$C_2F_6^+$	CF_3^+	14.43	1.54	0.09(0.02)	0.06(0.07)	>0.06	0.17
	$C_2F_5^+$	16.39	1.65	0.86(0.12)	0.52(0.06)	0.08	0.45
	$C_2F_5^+$	17.28	2.54	1.22(0.12)	0.48(0.05)	0.07	0.45
	$C_2F_5^+$	17.72	2.98	1.25(0.13)	0.42(0.04)	0.07	0.45
	$C_2F_5^+$	17.92	3.18	1.01(0.18)	0.32(0.06)	0.07	0.45
	CF_3^+	18.08	5.19	0.17(0.01)	0.03(0.04)	>0.06	0.17
	CF_3^+	21.01	8.12	0.49(0.06)	0.06(<0.01)	>0.06	0.17
	CF_3^+	21.94	9.05	0.69(0.07)	0.08(<0.01)	>0.06	0.17
$C_3F_8^+$	CF_3^+	14.03	1.07	0.09(0.03)	0.09(0.03)	>0.04	0.14
	CF_3^+	18.08	5.12	0.23(0.03)	0.04(0.01)	>0.04	0.14
	CF_3^+	21.94	8.98	0.43(0.09)	0.05(0.01)	>0.04	0.14
n-$C_4F_{10}^+$	CF_3^+	17.76	5.42	0.21(0.01)	0.04(<0.01)	>0.03	0.12
	CF_3^+	21.24	8.90	0.29(0.04)	0.03(0.01)	>0.03	0.12

[a] Method of analysis (Powis et al.[13]) assumes a two-body fragmentation. [b] Errors are given in parentheses.

than impulsive dissociation. A similar mechanism could also account for the production of $C_3F_6^+$ from n-$C_4F_{10}^+$. Note that the observation of CF_2^+ from C_2F_6 at an appearance energy as low as 14.0 eV, albeit with a low percentage branching ratio, also requires a fluorine anion to migrate.

In a previous RPD EI study on C_3F_8, Lifshitz et al.[24] noted that $C_2F_4^+$ has its first onset at 13.4 eV, which is 0.4 eV higher than that observed here. Our appearance energy of $C_2F_5^+$, 13.6 eV, is comparable to that recorded by Lifshitz et al.,[24] although slightly higher than the value of Noutary.[23] Neither of these results is particularly surprising. However, our appearance energy of CF_3^+ from C_3F_8 of 13.0 ± 0.1 eV (like $C_2F_4^+$, 0.4 eV lower than that recorded by Lifshitz et al.[24]) warrants further discussion because it relates to the ionization energy (IE) of the CF_3 radical. The dissociation energy of 12.96 eV (Table 2) for the production of $CF_3^+ + C_2F_5$ is calculated assuming the lowest value quoted in the literature for the heat of formation of CF_3^+ at 298 K, 360 kJ mol^{-1}, from a study of the $HCl^+ + CF_4$ ion−molecule reaction.[28] An upper limit for the IE(CF_3) of 8.64 eV was inferred. A later ion−molecule study of Kr^+ reacting with CF_4[30] measured an appearance energy of CF_3^+ from CF_4 at 298 K of 14.24 ± 0.07 eV, from which an IE(CF_3) of 8.62 ± 0.08 eV was inferred.[31] These values are substantially lower than the value of 9.25 eV assumed for many years from a PIMS study of CF_3[32] and are also much lower than a very recent ab initio calculation, 8.98 eV,[33] and a new evaluation, 9.05 eV, from a PIMS study of photofragmentation of C_2F_4.[31] The adiabatic IE of CF_3 is notoriously difficult to measure due to the change in geometry of the radical from pyramidal in its neutral form to planar in its ionized form, with a negligible Franck−Condon factor at threshold.[32,33] The CF_3^+ signal at 13.0 eV in our experiment cannot arise from second-order radiation because ionic states of C_3F_8 do not exist at 26 eV. Therefore, the presence of CF_3^+ from the fragmentation of C_3F_8 at 13.0 eV is strong evidence to support the low value for the IE(CF_3) of Tichy et al. and explains why we use this value in Table 2. (Inherent in this discussion, we have assumed that the errors in the heat of formation of C_3F_8 and C_2F_5 are negligible by comparison.) We have used the procedure of Traeger et al.[29] to convert our AE(CF_3^+/C_3F_8)$_{298}$ of 13.0 ± 0.1 eV into an upper limit for the heat of formation of CF_3^+ at 298 K of 383 ± 10 kJ mol^{-1}. This value uses the stationary electron convention for heats of formation of cations. Using the most accurate value available for the heat of formation of CF_3 at 298 K of −466 kJ mol^{-1},[31] we obtain an upper limit for the adiabatic IE of CF_3 of 8.8 ± 0.1 eV. A fuller account of this thermochemistry and possible causes for the discrepancy between our value of IE(CF_3) and that obtained by more direct methods such as PIMS[31,32] will be published elsewhere.[34]

For n-C_4F_{10}, a weak signal of $C_2F_4^+$ is also observed at threshold. As above, production of this fragment ion must involve F^- migration in the transition state to be thermodynamically feasible. $C_2F_5^+$ is also produced close to the onset of ionization and forms a substantial branching ratio in the range 13.0−16.4 eV. We have commented earlier that there are two types of C−C bond in n-C_4F_{10}, with an apparent extra feature in the TPES in this energy range. Therefore, the production of $C_2F_5^+$ could indicate impulsive fragmentation from a state of n-$C_4F_{10}^+$ produced by electron loss from an orbital associated with the middle C−C bond.

4.3.2. Fragmentation in the Range 15−24 eV. For the first excited state of $C_2F_6^+$ at 16.4 eV, the CF_3^+ signal decreases rapidly, with $C_2F_5^+$ becoming the dominant ion accounting for close to 100% of the branching ratio between 16 and 17 eV. The onset of $C_2F_5^+$, 15.4 ± 0.1 eV, corresponds (within experimental error) with the onset of the $\tilde{A}$ state of the ion. This suggests that $C_2F_5^+$ is produced directly from the $\tilde{A}$ state without prior internal energy conversion, in agreement with the conclusions of Inghram et al.[5] and Simm et al.[3,4] This phenomenon is characteristic of impulsive decay from an electronic state showing isolated-state behavior. To confirm this point, we have performed calculations to predict the breakdown diagram expected for a statistical mechanism. These calculations assume that the ground state of $C_2F_6^+$ is bound (which may be the case outside the Franck−Condon region), and vibrational frequencies from the neutral are inferred.[35,36] Figure 9a shows the percentage production of $C_2F_5^+$ at varying photon energies calculated by RRKM theory (section 3.1). The figure clearly shows that statistical theory cannot account for either the rapid turn-on or for the near 100% branching ratio of $C_2F_5^+$ observed between 16 and 17 eV in the breakdown diagram. The calculations show that CF_3^+ should be the dominant ion in this energy range. A similar situation is seen for $C_3F_8^+$ between 15.5 and 18.0 eV (Figure 2) with the formation of $C_3F_7^+$ being dominant. Since the maximum of $C_3F_7^+$ formation occurs at the same energy as a peak in the TPES at 16.5 eV, we again deduce that this behavior is characteristic of nonstatistical decay. As found for $C_2F_6^+$, RRKM calculations (using vibrational frequencies inferred from neutral C_3F_8[37]) cannot account for the high production rate of this fragment in favor of $C_2F_5^+$ or CF_3^+ over the energy range 16−18 eV. Results of these calculations are shown in Figure 9b. For n-C_4F_{10}, $C_4F_9^+$ is formed between 15.6 and 17.2 eV with a substantial branching ratio. Although RRKM calculations

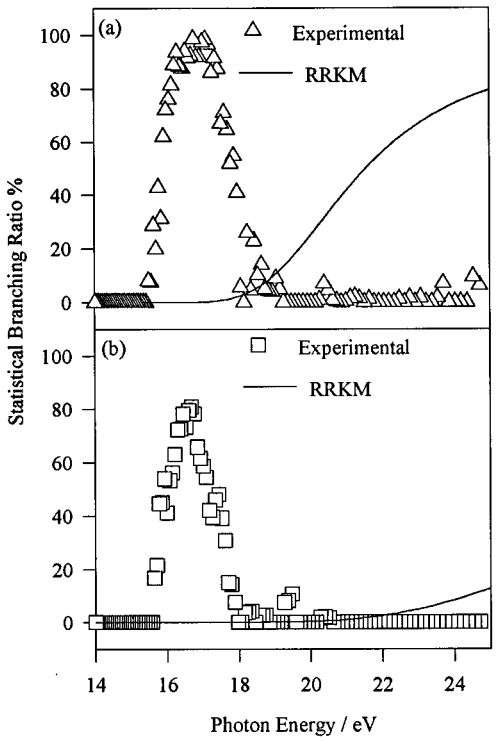

Figure 9. Experimental data and RRKM calculations of the percentage yield of (a) $C_2F_5^+$ from $C_2F_6^+$ and (b) $C_3F_7^+$ from $C_3F_8^+$ as a function of the photon energy. The figures show that $C_2F_5^+$ and $C_3F_7^+$ are only predicted to occur in negligible amounts over the energy range where they are experimentally observed.

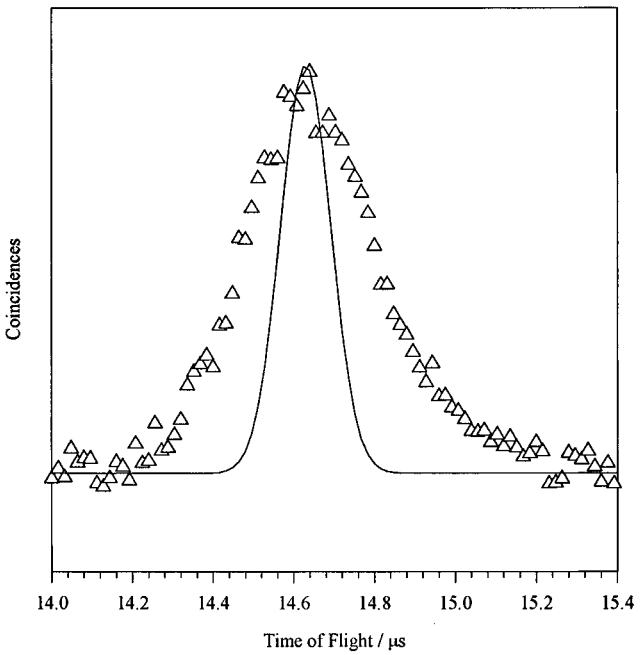

Figure 10. Coincidence time-of-flight spectrum (△) of CF_3^+ from C_3F_8 excited at 21.94 eV. The time resolution is 16 ns per channel. Analysis of the peak shape by the method of Powis et al.[13] yields $\langle E_T \rangle = 0.43 \pm 0.09$ eV. If CF_3^+ were to form as a parent ion at a temperature of 298 K, the shape of the peak (solid line) is predicted to be Gaussian with a width dependent on the mass of the ion (69 amu), the extraction field (20 V cm^{-1}), and the temperature.[39]

were not performed on this molecule due to lack of information on the vibrational frequencies, it seems highly unlikely that $C_4F_9^+$ can arise as a result of statistical decay.

The obvious consequence of decay over the energy range 15−18 eV being impulsive for all three species, and that similar products resulting from C−F bond breaking are observed, is that an electron is ejected from a C−F bonding orbital. As noted earlier, using CNDO molecular orbital calculations, the peak at 16.4 eV in the TPES of C_2F_6 has previously been assigned to removal of an electron largely associated with the π levels of the F atoms.[3] Our results suggest that the orbital probably has a substantial amout of C−F bonding character. This is in agreement with the suggestion by Brundle et al.[38] that perfluorination reduces the nonbonding character of all nonbonding electrons. The percentage yield of $C_2F_5^+$ does not recede until after the feature in the TPES of C_2F_6 at 17.2 eV. We have already proved that this peak arises due to autoionization; therefore, it would indicate that these Rydberg states are all autoionizing to the $\tilde{A}$ state.

For most of the ionic states above 18 eV, CF_3^+ is the major ion observed in all three molecules, and it is not immediately obvious whether decay is statistical or impulsive. For C_2F_6, the peak in the TPES at 18 eV has a threshold at around 17 eV with CF_3^+ becoming the dominant fragment ion. The rapid "switch on" of CF_3^+ with the equally rapid decline of $C_2F_5^+$ at an energy corresponding to state(s) of the parent ion possibly suggests impulsive behavior. It seems unlikely that CF_3^+ comes from dissociation of $C_2F_5^+$ since the total kinetic energy release is far smaller for CF_3^+ formation above 17 eV than it is for $C_2F_5^+$ formation around 17 eV. Further support for this was revealed by Inghram et al.,[5] who recorded time-dependent breakdown curves and discovered that $C_2F_5^+$ formed a small amount of CF^+ above 17 eV but no significant amount of CF_3^+. Our experiment gives no information on the neutral fragment(s) formed in association with CF_3^+ at these energies and on whether excited states are formed. Obviously, if excited states are involved, the fraction of the available energy appearing as kinetic energy of the products will be greater than the values given in Table 3. For C_2F_6 at ca. 24 eV, CF_2^+ is produced almost exclusively. Since CF_2^+ shows a rapid increase in signal at an energy corresponding to an ionic state in the TPES, it again suggests that impulsive behavior is taking place at these higher energies. For the other high-energy states around 21 eV, we cannot comment on the decay mechanism, except to note that these states fragment to CF_3^+.

4.4. Kinetic Energy Released in the Fragmentation of $C_2F_6^+$, $C_3F_8^+$, and n-$C_4F_{10}^+$. TPEPICO TOF spectra were measured at energies shown in Table 3 corresponding to some of the maxima seen in the TPES in Figures 1−3. In all cases, a TOF resolution of 16 ns per channel was used. As an example, Figure 10 shows the broadening of the CF_3^+ peak at a photon energy of 21.94 eV for C_3F_8. Measurements were not performed on $C_3F_7^+$ and $C_4F_9^+$ by fixed-energy TPEPICO for two reasons. First, the signals were weak on account of mass discrimination effects. Second, the unfavorable kinematics of these dissociation channels, with the much lighter fluorine atom produced as the other fragment, meant that the values of $\langle E_T \rangle$ would have a very large error. The table shows the experimentally determined mean total kinetic energy releases, $\langle E_T \rangle$, as well as the theoretically calculated fractional releases for both pure impulsive and statistical decay (section 3). For the breakup of $C_2F_6^+$ into $C_2F_5^+ + F$, the fraction of energy released into translation is satisfactorily modeled by the pure impulsive model. Our results are in excellent agreement with those of Simm et al.[4] and Inghram et al.[5] and are also expected from the earlier conclusions drawn from the breakdown diagram (section 4.3). On the other hand, the values of $\langle E_T \rangle$ for the formation of CF_3^+ from $C_2F_6^+$, $C_3F_8^+$, and n-$C_4F_{10}^+$ over a wide range of energies suggest a statistical decay mechanism is

operative. As mentioned earlier, however, a low fractional KE release does not necessarily imply statistical decay, and fragmentation from the ground state of $C_2F_6^+$, $C_3F_8^+$, and n-$C_4F_{10}^+$ is likely to be impulsive since these states are repulsive in the Franck−Condon region. This is therefore an indication that one or both of the resulting fragments from $C_2F_6^+$, $C_3F_8^+$, and n-$C_4F_{10}^+$ are left with a large amount of vibrational excitation caused by an intrafragment mechanism. The most likely candidate for CF_3^+ is the out-of-plane bending umbrella mode (ν_2), due to the CF_3 group being pyramidal in the neutral PFC while CF_3^+ is planar. There is then a large change in the degree of planarity of the receding fragments in the impulsive fragmentation. Fluorination is known to cause delocalization of the σ molecular orbitals,[38] a trait which makes PFCs extremely stable as neutral species. On removal of an electron, the stability of the species is reduced, and it seems likely that both the C−C and C−F bond lengths may increase. The higher energy states of $C_2F_6^+$ etc. at energies greater than 18 eV also dissociate primarily to CF_3^+. Whether these states decay statistically or impulsively is difficult to ascertain from the KE data, since the low fractional KE releases can be accounted for by both mechanisms.

We note that Inghram et al.[5] performed field ionization experiments on C_2F_6 and showed that both the CF_3^+ and $C_2F_5^+$ fragments were formed in a short time corresponding to only one vibrational period (5×10^{-13} s). Unfortunately, the energy range over which these experiments were carried out was not defined, and therefore they cannot be directly related to decay of $C_2F_6^+$ into $CF_3^+ + CF_3$ above or below the $\tilde{A}\ ^2E$ state.

5. Conclusions

We have recorded TPEPICO spectra of C_2F_6, C_3F_8, and n-C_4F_{10} continuously as a function of energy and over a much wider energy range (12−25 eV) than has previously been reported. Two important thermochemical results from the C_3F_8 study have been obtained; the adiabatic IE of CF_3 is less than or equal to 8.8 ± 0.1 eV, in good agreement with values obtained from two ion−molecule studies,[28,30] and the heat of formation of $C_3F_7^+$ at 298 K is less than or equal to −360 ± 20 kJ mol^{-1}.

As was inferred by Lifshitz and Long[2] for $C_2F_6^+$ and $C_3F_8^+$ from mass spectrometric data, impulsive behavior has been observed for all three molecules for their cationic states below 18 eV. This allows some deductions about the types of electrons removed in the formation of the ionic states to be made. This behavior seems quite remarkable considering the number of atoms that are present for the longer-chain species. The consequence of impulsive behavior must be that the majority of states observed are unbound in the Franck−Condon region, resulting in decay on a time scale comparable to or faster than vibrational motion. This study also indicates that a consequence of perfluorination is that all electrons are delocalized to some extent. For example, F 2pπ nonbonding electrons are also partially C−F bonding, causing C−F breakage upon electron removal from this orbital.

There is some evidence that as the size of the molecule increases, the extent of impulsive behavior reduces. For example, for the C−F bond-breaking channel to form $C_2F_5^+$, $C_3F_7^+$, and n-$C_4F_9^+$, the maximum branching ratio decreases from ca. 100% for $C_2F_6^+$ to ca. 60% for n-$C_4F_{10}^+$. This may indicate that as the size of the parent ion increases there are more surrounding states smearing out the impulsive behavior of the state under study or that statistical behavior is taking over. If the latter situation is true, the increased density of states as the size of the ion increases means that energy randomization between the states is more likely, allowing the ion to be slightly longer lived.

From the kinetic energy measurements, it is apparent that decay of $C_2F_6^+$ to form $C_2F_5^+ + F$ is taking place impulsively. Results on the CF_3^+ fragment are less conclusive since only small kinetic energy releases are observed. Since previous studies on the decay of $C_2F_6^+$ suggests that decay to $CF_3^+ + CF_3$ is indeed a rapid process taking place in less than the time for one vibration,[5] the low fractional KE result indicates that on breakup one or both of the departing species are formed with a large amount of vibrational energy.

Acknowledgment. We thank NERC, EPSRC, and the Daresbury Laboratory for a Research Grant, Research Studentships (G.K.J., K.J.B.), and a CASE award (K.J.B.). We also thank Dr. I. Powis (Nottingham University) for the use of his kinetic energy analysis program and Dr. P. A. Hatherly (Reading University) for technical advice on the apparatus.

References and Notes

(1) Marcus, R. A.; Rice, O. K. *J. Phys. Colloid Chem.* **1951**, *55*, 894. Marcus, R. A. *J. Chem. Phys.* **1952**, *20*, 359.
(2) Lifshitz, C.; Long, F. A. *J. Phys. Chem.* **1965**, *69*, 3746.
(3) Simm, I. G.; Danby, C. J.; Eland, J. H. D. *Int. J. Mass Spectrom. Ion Phys.* **1974**, *14*, 285.
(4) Simm, I. G.; Danby, C. J.; Eland, J. H. D.; Mansell, P. I. *J. Chem. Soc., Faraday Trans. 2* **1976**, *72*, 426.
(5) Inghram, M. G.; Hanson, G. R.; Stockbauer, R. *Int. J. Mass. Spectrom. Ion Phys.* **1980**, *33*, 253.
(6) Smith, D. M.; Tuckett, R. P.; Yoxall, K. R.; Codling, K.; Hatherly, P. A.; Aarts, J. F. M.; Stankiewicz, M. *J. Chem. Phys.* **1994**, *101*, 10559.
(7) Prasil, Z.; Forst, W. *J. Phys. Chem.* **1967**, *71*, 3166. Stockbauer, R. *J. Chem. Phys.* **1973**, *58*, 3800.
(8) Güthe, F.; Weitzel, K. M. *Ber. Bunsen-Ges. Phys. Chem.* **1997**, *101*, 484.
(9) Jarvis, G. K.; Boyle, K. J.; Mayhew, C. A.; Tuckett, R. P. *J. Phys. Chem. A* **1998**, *102*, 3230.
(10) Hatherly, P. A.; Stankiewicz, M.; Codling, K.; Creasey, J. C.; Jones, H. M.; Tuckett, R. P. *Meas. Sci. Technol.* **1992**, *3*, 891.
(11) Hatherly, P. A.; Smith, D. M.; Tuckett, R. P. *Z. Phys. Chem. (Munich)* **1996**, *195*, 97.
(12) Wiley, W. C.; Maclaren, I. H. *Rev. Sci. Instrum.* **1955**, *26*, 1150.
(13) Powis, I.; Mansell, P. I.; Danby, C. J. *Int. J. Mass Spectrom. Ion Phys.* **1979**, *32*, 15.
(14) Creasey, J. C.; Jones, H. M.; Smith, D. M.; Tuckett, R. P.; Hatherly, P. A.; Yoxall, K. R.; Codling, K.; Powis, I. *Chem. Phys.* **1993**, *174*, 441.
(15) Eland, J. H. D. *Photoelectron Spectroscopy*, 2nd ed.; Butterworth: London, 1984.
(16) Creasey, J. C.; Smith, D. M.; Tuckett, R. P.; Yoxall, K. R.; Codling, K.; Hatherly, P. A. *J. Phys. Chem.* **1996**, *100*, 4350.
(17) Whitten, G. Z.; Rabinovitch, B. S. *J. Chem. Phys.* **1963**, *38*, 2466.
(18) Klots, C. E. *J. Chem. Phys.* **1973**, *58*, 5364.
(19) Illenberger, E.; Momigny, J. *Gaseous Molecular Ions*; Springer-Verlag: New York, 1992.
(20) Busch, G. E.; Wilson, K. R. *J. Chem. Phys.* **1972**, *56*, 3626. Riley, S. J.; Wilson, K. R. *Discuss. Faraday Soc.* **1972**, *53*, 132.
(21) Mitchell, R. C.; Simons, J. P. *Discuss. Faraday Soc.* **1967**, *44*, 208.
(22) Note that the observed onset of ionization in these molecules only provides an upper limit for the adiabatic ionization potential. The reason for this is that the ground states of $C_2F_6^+$ etc. are repulsive in the accessible Franck−Condon region, as evidenced by the absence of parent ion signal in the TPEPICO spectra.
(23) Noutary, C. S. *J. Res. NBS* **1968**, *72A*, 479.
(24) Lifshitz, C.; Grajower, R. *Int. J. Mass Spectrom. Ion Phys.* **1969**, *3*, 211.
(25) Lias, S. G.; Bartmess, J. E.; Liebman, J. F.; Holmes, J. L.; Levin, R. D.; Mallard, W. G. *J. Phys. Chem. Ref. Data, Suppl. 1* **1988**, *17*.
(26) Bryant, W. M. *J. Polym. Sci.* **1962**, *56*, 278.
(27) Su, T.; Kevan, L.; Tiernan, T. O. *J. Chem. Phys*. **1971**, *54*, 4871.
(28) Tichy, M.; Javahery, G.; Twiddy, N. D.; Ferguson, E. E. *Int. J. Mass Spectrom. Ion Phys.* **1987**, *79*, 231.
(29) Traeger, J. C.; McLaughlin, R. G. *J. Am. Chem. Soc.* **1981**, *103*, 3647.
(30) Fisher, E. R.; Armentrout, P. B. *Int. J. Mass Spectrom. Ion Processes* **1990**, *101*, R1.

(31) Asher, R. L.; Ruscic, B. *J. Chem. Phys.* **1997**, *106*, 210.
(32) Lifshitz, C.; Chupka, W. A. *J. Chem. Phys.* **1967**, *47*, 3439.
(33) Horn, M.; Oswald, M.; Oswald, R.; Botschwina, P. *Ber. Bunsen.-Ges. Phys. Chem.* **1995**, *99*, 323.
(34) Jarvis, G. K.; Tuckett, R. P. *Chem. Phys. Lett.*, in press.
(35) Nielson, J. R.; Richards, C. M.; McMurry, H. L. *J. Chem. Phys.* **1948**, *16*, 67.
(36) Mills, I. M.; Person, W. B.; Scherer, J. R.; Crawford, B. *J. Chem. Phys.* **1957**, *28*, 51.
(37) Edgell, W. F.; Mallory, H. D.; Weiblen, D. G. *J. Am. Chem. Soc.* **1950**, *72*, 4856.
(38) Brundle, C. R.; Robin, M. B.; Kuebler, N. A.; Basch, H. *J. Am. Chem. Soc.* **1972**, *94*, 1451.
(39) Franklin, J. L.; Hierl, P. M.; Whan, D. A. *J. Chem. Phys.* **1967**, *47*, 3184.